Sheffield
Hallam
University

Tribological properties and wear mechanisms of DC pulse plasma nitrided austenitic stainless steel in dry reciprocating sliding tests

LUO, Quanshun <http://orcid.org/0000-0003-4102-2129>, OLUWAFEMI, Oluwaseun, KITCHEN, Matthew and YANG, Shicai

Available from Sheffield Hallam University Research Archive (SHURA) at:

http://shura.shu.ac.uk/14255/

This document is the author deposited version. You are advised to consult the publisher's version if you wish to cite from it.

Published version

Repository use policy

Sheffield Hallam University Research Archive
http://shura.shu.ac.uk

Tribological properties and wear mechanisms of DC pulse plasma nitrided austenitic stainless steel in dry reciprocating sliding tests

Quanshun Luo[1*], Oluwaseun Oluwafemi[1], Matthew Kitchen[1], Shicai Yang[2]

[1]Materials and Engineering Research Institute, Sheffield Hallam University, Howard Street, Sheffield S1 1WB, UK

[2]Teer Coatings Ltd., Miba Coating Group, West Stone House, Berry Hill Industrial Estate, Droitwich, WR9 9AS, UK

Abstract

Expanded austenite (γ_N), or S-phase, is a special phase of low-temperature nitrided austenite containing highly super-saturated nitrogen in the form of heterogeneous Cr-N nano-clusters. A nitrided layer of singe phase γ_N is known to provide austenitic stainless steel with combined high hardness, good wear resistance and superior corrosion resistance. This paper reports recent experiments on a comparative study of the sliding wear properties and wear mechanisms of nitrided austenite stainless steel AISI 316, with a special attention paid on worn surface structural evolutions induced by frictional heating and sliding deformation. The samples were prepared by DC pulsed plasma nitriding treatments of various time at a fixed power. Knoop micro-indentation has revealed hardening behaviour of the nitrided samples. The reciprocating ball-on-disc sliding wear and friction properties were investigated at ambient environment conditions using an alumina counterpart ball. The worn surfaces have been analysed by XRD,FEG-SEM and EDX to show wear induced changes in the crystalline characteristics and the wear mechanisms of tribo-oxidation, cracking, abrasive wear and ploughing deformation. Moreover, longitudinal cross-sectional foils of the worn samples have been prepared and analysed using TEM, to investigate the wear induced structural changes, including tribofilm formation, plastic deformation and delamination in depths of nano-scale.

Key words: Expanded austenite; DC pulsed plasma nitriding; Ball-on-disc sliding wear; Wear mechanisms; Cross-sectional TEM; Quantitative X-ray diffraction

1 Introduction

Austenitic stainless steels have many important industrial applications owing to their excellent corrosion resistance [1]. The corrosion resistance is attributed predominantly to the sufficiently high chromium concentration in the matrix, whereas the high nickel content helps stabilize the austenitic lattice structure. However, these steels may suffer from severe wear failures because of the low hardness and good plasticity of the austenitic matrix. It is well known that nitriding is an effective way to harden the surface of austenitic stainless steel and to improve the wear resistance. It has been revealed that the microstructure of a nitrided layer depends strongly on the kinetic nitriding process, especially the processing temperature [2-4]. In particular, conventional nitriding at temperatures exceeding 500 ºC is able to obtain a thick nitrided layer of high hardness, whereas the massive precipitation of chromium nitride deteriorates the corrosion resistance because of the resultant depletion of chromium in the ferrous matrix[5].

In middle 1980's, a few research groups reported that, by lowering the process temperature to about 400 ºC, a CrN-free nitrided layer could be produced to have combined high hardness and excellent corrosion resistance [4-6]. Soon after that, extensive research has been undertaken worldwide to characterize the precipitate-free nitrided surfaces. A recent review paper about structural characterization of nitrided austenitic stainless steels can be found in Ref [7]. Early X-ray diffraction (XRD) analyses revealed its single-phase nature, severe lattice distortion, and extremely large lattice expansion as compared to the normal austenite phase, as well as a tetragonal lattice similar to martensite [4, 8-11]. According to the findings of different researchers, the unknown

phase was named as 'S-phase', 'expanded austenite' or 'N-expanded solid solution (γ_N)', or 'm-phase'. X-ray photoelectron spectroscopy analyses showed preferential Cr-N bonds in the γ_N layers [12, 13]. More recently, multi-technical experimental analyses, by means of XRD, field emission microscopy, conversion electron Mossbauer, X-ray absorption near edge structure and extended X-ray absorption fine structure spectroscopes, and atomic probe tomography, showed that the XRD homogeneous expanded austenite phase is microscopically heterogeneous because of the different electronic structures of the Fe, Cr and Ni components [14, 15]. Consequently the structure of the γ_N phase has been found to consist of nanoscale CrN precipitates dispersed in an N-saturated Fe_4N-like matrix. In particular, the N-expanded austenite was found to comprise dispersive CrN^{2+} molecular ions, at a spacing of approximately 4.5 nm. In thermodynamics, on the other hand, the meta-stable γ_N phase is expected to transform to CrN and γ'-Fe_4N precipitates embedded in a low-nitrogen ferrous matrix which are thermodynamically more stable. Such transformation occurs not only in the nitriding processes at higher temperatures, e.g. above 500 ^{0}C, but also in a nitrided steel when it was annealed at high temperatures [16]. Moreover, dry sliding is known to generate frictional heat which, when the resultant flash temperature is sufficiently high, may bring about local structural evolution of the γ_N phase in a nitrided layer. Provided that current understanding on the wear and friction mechanisms has been progressed to atomic and nano scales of materials interactions, such structural changes cannot be ignored.

Up to date, most of the tribological research on nitrided austenitic stainless steels has been mainly focused on their wear and friction properties as compared to those of non-nitrided samples, although limited results were also published on the wear mechanisms. Sun and Bell investigated the sliding wear behaviours of 316 austenitic stainless steel samples being nitrided at three temperatures between 450 ^{0}C - 550 ^{0}C [17]. They found that, all the nitrided surfaces exhibited substantially lower wear rates than the 316 steel when the sliding was against a hardened steel or alumina ball counterpart, while the 450 ^{0}C nitrided sample showed the best wear performance. Comparative tribological tests against a WC counterpart obtained similar results, whereas the increased wear resistance of the nitrided surfaces were attributed to a transition of wear mechanism from adhesive wear with severe plastic deformation to mild wear modes of abrasion and tribo-oxidation [18]. Lei and co-workers studied the lubricated sliding wear of an austenitic stainless steel sample after ion nitriding treatment at 380 ^{0}C, in which they found that, the ion nitriding could significantly improve the abrasive resistance [19]. In another paper [20], the authors investigated the rolling-sliding wear behaviour and wear mechanisms of nitrided austenitic stainless steel sample, which revealed delamination wear in the nitrided surfaces as a result of severe plastic deformation. Similar tribological studies were also published by other researchers [21-23]. Nevertheless, there is still lack of knowledge on wear failure mechanisms of nitrided austenitic steels, especially on the nano-scale materials failures including any friction induced structural evolution on the worn surface.

In this paper, we report original experiment results of reciprocating sliding wear tests of plasma nitrided austenitic stainless steel. The samples were treated at various times from 10 to 240 minutes in a pulsed plasma nitriding process to obtain different thickness and different microstructure of the nitrided case. In addition to the effect of nitriding time on the wear and friction properties, detailed wear and friction mechanisms have been studied by scanning electron microscopy (SEM) and cross-sectional transmission electron microscopy (TEM). The frictional heating induced structural changes in the nitrided cases have also been investigated by quantitative X-ray diffraction (XRD).

2 Experimental

2.1 Sample materials

The sample steel was an austenitic stainless steel AISI 316. Square sheets were ground and polished using 1200# SiC abrasive papers to final dimensions of 20 mm in length and 2 mm in thickness, and ultrasonically cleaned for 10 minutes in acetone.

Nitriding treatments were carried out using a high power pulsed glow discharge plasma (HPPGDP), being generated in a cylindrical vacuum chamber of 550 mm in diameter and 600 mm in height. The samples were fixed on the substrate turntable of 350 mm in diameter. The turntable was biased by a HPPGDP power generator (AE Pinnacle™ Plus) with parameters of power up to 6.0 kW (equivalent to a maximum power density of 2.0 W/cm^2 or current density of 3.3 mA/cm^2 on substrate), frequency up to 350 kHz, positive going pulse width up to 1600 ns, implying a duty cycle of 44%, and an adjustable negative bias potential as low as -600V. Details of the plasma nitriding process can be found in a recent publication [24]. In this experiment, the samples were prepared

using a HPPGDP process with the parameters: pressure 1.33 Pa of mixed Ar and N_2 gases at a constant flow ratio of 1:2, plasma power 2.5 kW and various process times of 10, 30, 60, 90, 120, 180 and 240 minutes.

2.2 Mechanical and tribological testing

Knoop indentation was made on a Mitutoyo MVK H2 microhardness tester to measure the hardness of the as-nitrided surfaces. An indenting load of 0.025 kg, i.e. 0.245 N, was applied. Each average value was obtained from measurements of five indents.

A computer-controlled multi-functional tribometer (CERT-UMT-2, USA) was employed to carry out the reciprocating sliding wear tests. An alumina ball of 6 mm in diameter was used as the counterpart to slid on the nitrided discs. The tribotests were conducted at room temperature in ambient conditions and under a constant normal load of 0.5 kg, or 4.9 N, a reciprocating sliding length of 8.0 mm, and a selected nominal sliding speed of 0.02 m·s^{-1}. Under the selected reciprocating length and sliding speed, the actual reciprocating frequency was measured to be 47 passes per minutes. Each test took a sliding period of 30 minutes. Therefore, the total reciprocating passes and sliding distance were calculated to be 1410 passes and 11.28 m respectively.

After each tribotest, the wear coefficients of both the disc sample and the counterpart ball were measured. The wear coefficient was calculated as the volume per applied load (unit: N) per sliding distance (unit: m). For the disc sample, the tested sample was cleaned by wet sweeping using cotton and acetone to remove loose wear debris. Then three cross-sectional scans of the wear track were made on a 3D profilometer (alicona Infinite Focus Microscope (IFM), Alicona Imaging GmbH, Austria) to measure the linear profile and thereafter to determine the wear properties, including average and maximum depths, cross-sectional worn area and wear volume.

For the counterpart ball, the loose wear debris attached on the wear scar was cleaned using a clean soft tissue before the ball, being still fixed in the holder, was taken to an optical microscope to measure the diameter of the resultant wear scar. The ball wear volume, V, was calculated using the following formula.

$$V = \pi \cdot h^2 \cdot (R^2 - h/3) \tag{1}$$

$$h = R - \sqrt{(R^2 - r^2)} \tag{2}$$

where R and r stand for the radius of the ball, 3.0 mm, and the wear scar respectively, and h is an intermediate parameter standing for the height of the worn ball segment.

2.3 Characterisation of as-nitrided and wear-tested samples

A field emission gun scanning electron microscope, FEI Nova200 FEG-SEM, was employed to observe the nitriding induced morphological changes of the sample surfaces and the worn surfaces. Moreover, vertical cross-sectional metallographic specimens were prepared to observe the microstructure and case depth of each nitrided sample.

After the wear tests, a longitudinal cross-section of a tested specimen was prepared in exactly the middle width of a selected wear track, to investigate the wear induced mechanical and microstructural changes in certain depth. The specimen was carefully cut using a SiC disk saw, and manually ground, polished, and chemically etched before SEM observation. After that, grinding and polishing were undertaken on the other side of the specimen to a final thickness of 40 µm. Then it was further thinned by means of ion beam polishing using a Precision Ion Polishing System (PIPS, Gatan 691, USA) to the thickness of electron transparency. The prepared thin foil was observed on a transmission electron microscope (Philips CM20 STEM), working at 200 kV and with a LaB_6 filament and with a digital camera.

A Co-tube Empyrean X-ray diffractometry (PANalytical B.V., Netherlands), being powered at 40 kV and 40 mA to emit X-ray K_{α}-Co of λ = 0.1789 nm, was employed to characterise the crystallographic properties of the nitrided samples as well as the sliding wear induced crystallographic changes on selected samples. For the latter, precise calibration was made to ensure the incident X-ray beam was focused well inside the wear track. Each XRD scan was performed to cover a range of diffraction angle of 2θ = 30º - 100º, at a step size of 0.026º and nominal time per step of 250 seconds. After stripping the $K_{\alpha 2}$ (λ = 0.1793 nm) and removing the background, a self-developed Gaussian multiple peak fitting process was applied to resolve the diffraction peaks, from which the detailed crystalline structure of each nitrided layer could be determined. The principle and analytical method of the Gaussian peak fitting process can be found in recent publications [25, 26].

3 Results and discussion

3.1 Effect of nitriding time on the hardness, thickness and surface morphology of nitrided cases

Fig. 1 shows variation of sample surface morphology with increasing nitriding time. After up to 30 minutes of nitriding treatment, the sample surface remains smooth, whereas ion bombarding induced marks are visible in sub-micron scale, as seen in Fig. 1a and its insert. When the nitriding time was increased to 60 minutes, the nitrided surface shows such a morphology that reflects the granular austenite microstructure of the steel, seeing the grain boundaries (labelled as 'G.B.') in Fig. 1b. In addition, deformation slips and twins appear inside some grains. Similar features were described in literature as micro-twins and slip bands as a result of plastic deformation [5, 27, 28]. At higher magnification, each slip band between two deformation slips exhibits a dense and uniform distribution of fine slip bands, indicating occurrence of slipping deformation along certain crystalline planes. When the nitriding time was increased to 90 minutes and longer, the surfaces became even rougher by showing a clear three-dimensional granular image in each case. Every grain, as being observed at high magnifications, shows dense packing of slipping bands. Regarding the tribotests, such variation of surface roughness is expected to influence the friction and wear behaviour.

Fig. 2 shows the effects of nitriding time on the hardness and thickness of the resultant case layer. Whereas the nitriding induced structural change and hardening are very marginal in the first 30 minutes, the nitrided case was measured to be 4.7 μm in the 60 minute nitrided sample which shows a surface hardness of $HK_{0.025}$ 1212 ± 225. More pronounced nitriding is seen to take place when the nitriding time was 90 minutes and longer, in which the case depth became 15 - 25 μm and the surface hardness was increased to close to or higher than
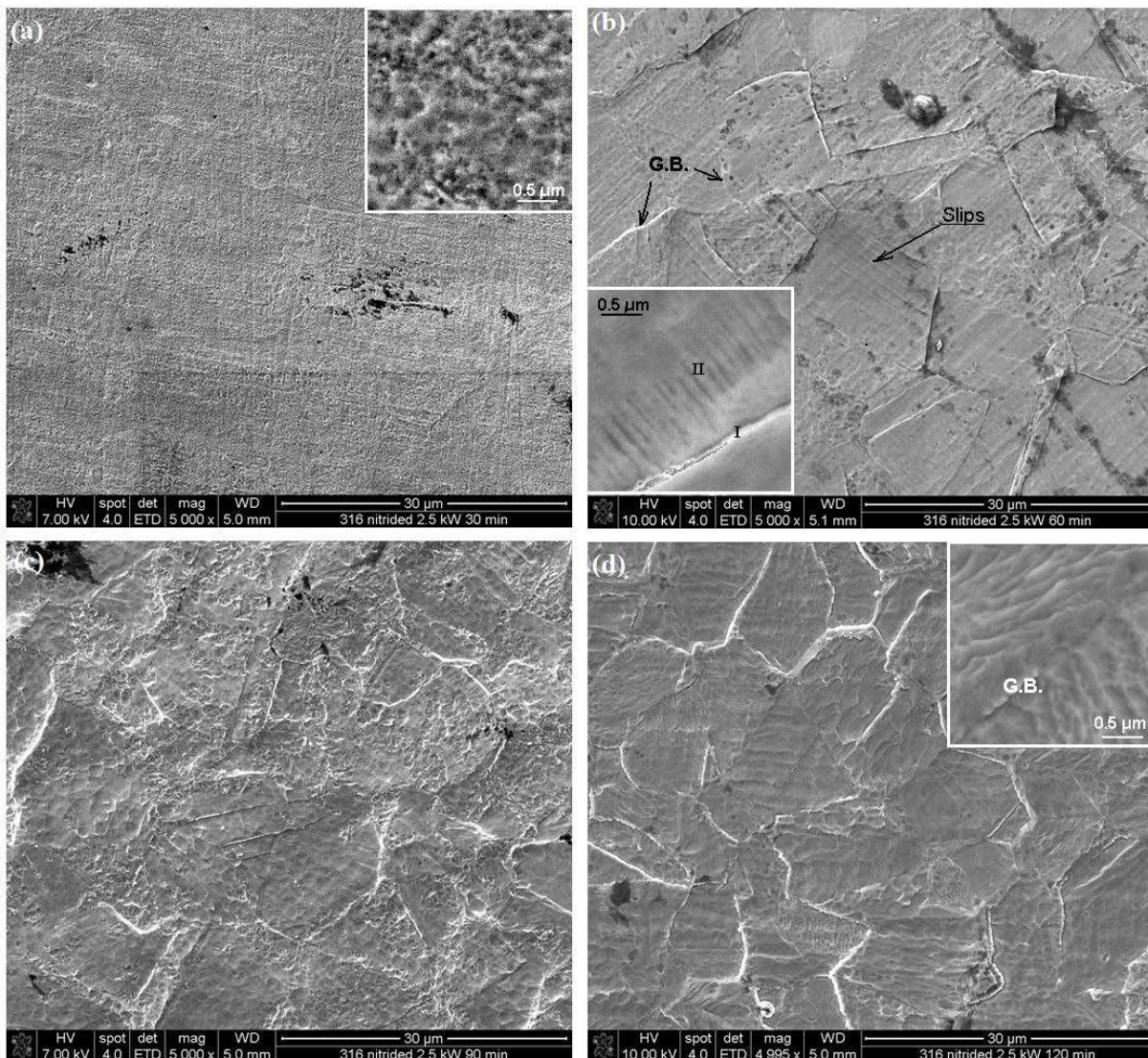

Figure 1 SEM micrographs of the sample surfaces after different time of nitriding treatment: (a) 30 min; (b) 60 min; (c) 90 min; and (d) 120 min.
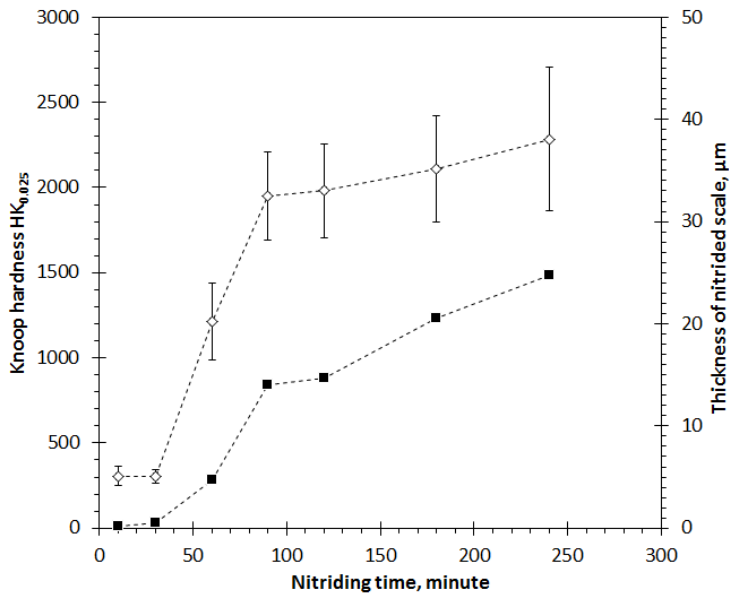
Figure 2 Effect of nitriding time on the surface hardness and the thickness of nitrided scale.
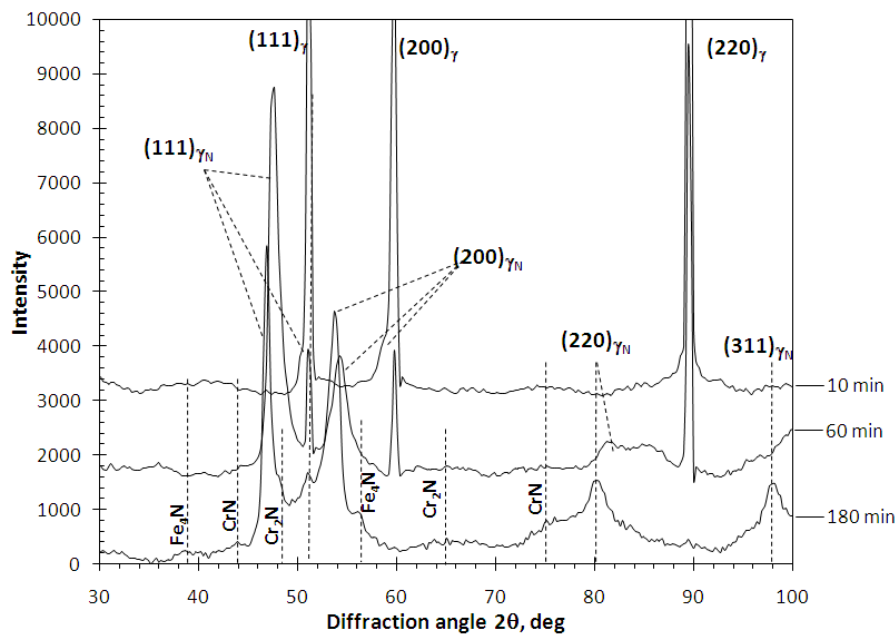

Figure 3 X-ray diffraction curves of the nitrided surfaces after three different nitriding times.

$HK_{0.025}$ 2000. The large scattering in the hardness values was due to the increased surface roughness which strongly influenced the shape and dimension of the resultant Knoop indents.

3.2 X-ray diffraction analyses of as-nitrided and wear-tested samples

Fig. 3 shows the XRD curves of the as-nitrided samples, to show the effect of nitriding time on the X-ray diffraction results. The lattice parameters of the expanded austenite γ_N phase and the substrate austenite γ are listed in Table 1, which were determined using the diffraction peaks from (111) up to (311) planes.

The diffraction curve of the 10 minute nitrided surface exhibits predominantly the austenite peaks of the substrate, indicating very marginal nitriding. Even that, the (111) and (200) peaks both show a low and broad shoulder at their left hand side, suggestive of the presence of a thin γ_N layer. The γ_N layer shows slightly expanded lattice with a small expansion ratio of only 1.3%.

The results in Figs. 1-3 reveal that a short-period nitriding treatment less than 60 minutes did not produce a significant nitrided case thickness. As a result, the friction and wear of the 10- and 30 minute nitrided samples reflected generally the sliding behaviours of the austenitic stainless steel substrate, which is beyond the scope of this paper and therefore is not investigated further.

The 60 minute nitrided sample shows predominantly the diffractions of the γ_N phase, especially the (111) and (200) peaks of substantial expansion. The γ_N and γ phases have lattice parameters of 0.3881 nm and 0.3591 nm, respectively, leading to a linear expansion ratio of 8.1%. The 180 minute nitrided sample recorded weak diffractions of CrN, Fe_4N and Cr_2N in addition to the γ_N phase, which indicates nitride precipitates.

Table 1 Lattice parameter of austenite (γ) and expanded austenite (γ_N)

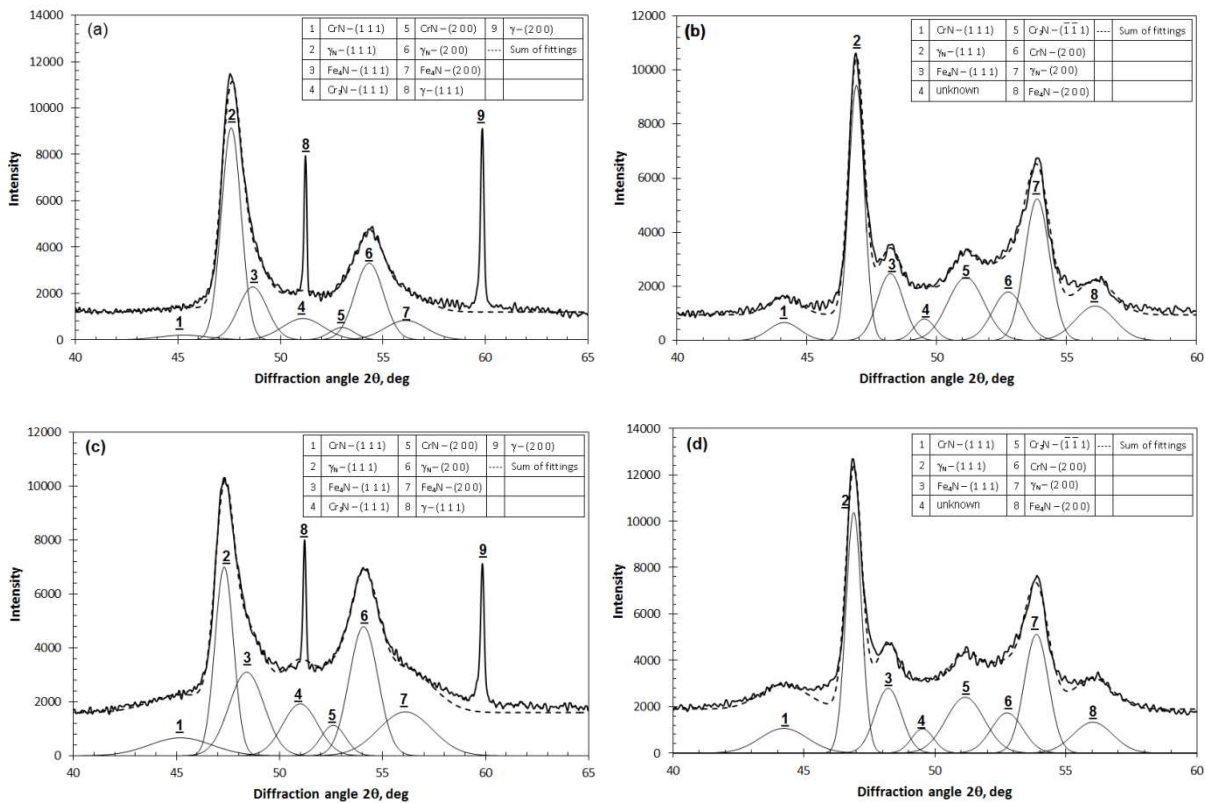| Nitrided time	γ [nm]	γN [nm]	ε [%]
10 min	0.3592	0.3635	1.3
60 min	0.3591	0.3881	8.1
180 min	-	0.3929	9.4

Figure 4 XRD curves and the associated Gaussian fittings of diffraction peaks: (a) on the 60 minute as-nitrided surface; (b) on the 240 minute as-nitrided surface; (c) on the worn surface of the 60 minute nitrided sample; and (d) on the worn surface of the 240 minute nitrided sample.

In Fig. 4, quantitative diffraction analyses were carried out on two nitrided samples to study the crystallographic characteristics of the nitride precipitates, where a Gaussian multi-peak fitting method has been applied to fit all the diffraction peaks. The diffraction curves in Fig. 4a and 4b were acquired on the as-nitrided surfaces of the 60 minute and 240 minute nitrided samples, respectively. In every diffraction curve, all the diffraction peaks have been fitted using a recently developed multiple Gaussian peak-fitting technique. More details of the method have been published elsewhere [25, 26].

It can be found that, each diffraction curve fits well to the γ_N phase, the substrate austenite and three types of nitride precipitates. In particular, even the 60 minute nitrided sample has shown the presence of three types of nitride precipitates, namely Fe_4N, CrN and Cr_2N, although these precipitates were not visible when the sample was observed using OPM, SEM and even TEM. It is also noticed that, all the nitride diffraction peaks exhibit super broadening, which implies extremely small grain sizes [3, 27-29].

The dimensions of the nitride precipitates have been estimated, according to the peak broadening, to be only 3 - 7 nm approximately as short-range ordered domains. As compared to literature [7-11], the current analysis has provided a closer view of the atom stacking structure of the γ_N phase. The detected short-range ordered domains are consistent to the results of other researchers that, nano-scale Cr-N and Fe-N clusters can be formed in the expanded austenite phase due to the preferential chemical bonds of nitrogen to the Cr and Fe atoms [12-15].

The Gussian-fitted peaks have been quantified to calculate the relative ratios of integrated peak intensity. The results are shown in Fig. 5. In the 60 minute nitrided sample, the γ_N-(111) and γ_N-(200) planes account for 64.2% of the total integrated intensity, whereas the rest intensity derives from five peaks of the three nitrides of CrN, Fe_4N and Cr_2N. In contrast, the γ_N phase of the 240 minute nitrided surface shows increased relative intensity in most of the nitride diffraction peaks, indicating pronounced nitride precipitation with increasing nitriding time.

In addition, the same XRD acquisition has been undertaken, after the wear tests, inside the wear tracks of the two samples in order to detect any crystalline structural change induced by the sliding wear. The results are shown in Fig. 4c and 4d, respectively. Again, the obtained XRD curves fit well to the three nitride precipitates as well as the γ_N phase.
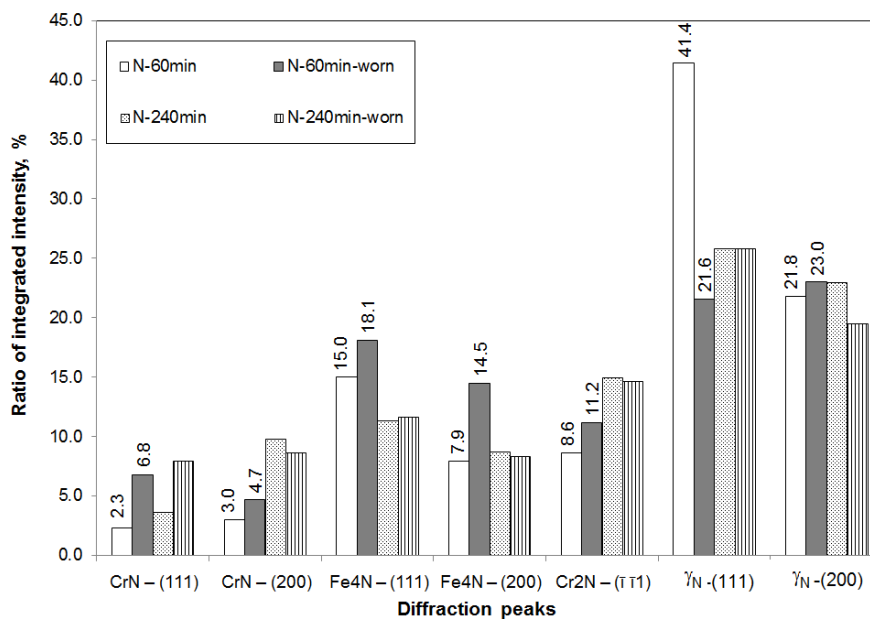

Figure 5 Effect of nitriding time and sliding wear on the relative diffraction intensity of the nitride precipitates and expanded austenite. Note the increased intensity of nitride precipitates of the 60 minute nitrided sample as a result of the sliding wear.

Moreover, it is interesting to note that, the applied sliding wear exhibits different influence on the two nitrided samples in term of the amount of the nitride precipitates. In the 240 minute nitrided sample, the relative intensities of the three nitride precipitates remain comparable between the as-nitrided and the wear-tested areas, Figure 5. It is known that, frictional heat is generated in dry sliding contact, whereas a high flash temperature is achieved at very close vicinity of the sliding surface depending on the severity of friction and the sliding speed [32-34]. The comparable amount of nitride precipitates suggests that the developed nitrided case was thermally stable. In the 60 minute nitrided sample, on the other hand, the worn surface shows increased intensity of the three precipitates (Fig. 5), which suggests more nitride precipitates in the worn surface than in the as-nitrided area. The increased precipitates imply that the applied sliding wear triggered decomposition of the expanded austenite phase at the upmost worn surface. Similar decomposition has been found when a low-temperature nitrided sample was annealed at a high temperature [16].

3.3 Friction behaviour

Fig. 6 shows the friction curves of the nitrided samples. A running-in period appeared in the beginning of each test before it reached a steady-state friction. In the sample being nitrided for 240 min, the friction started from low initial friction, and increased gradually to the steady state after approximately 5 minutes. The rest of the samples, on the other hand, exhibited high values of initial friction coefficient before the coefficients dropped to

the steady state. It is known that running-in is a special period of sliding that the friction and wear behaviour depends on several factors, which was not the main focus of the current study. Our previous research has suggested that, the variation of friction in a running-in period is caused by the generation of initial wear debris and its subsequent mechanical, thermal and tribo-chemical interactions between the sliding couple surfaces when the debris is engaged in the sliding contact to lead to the formation of an adhesive tribofilm attached on the worn surface [35-37].
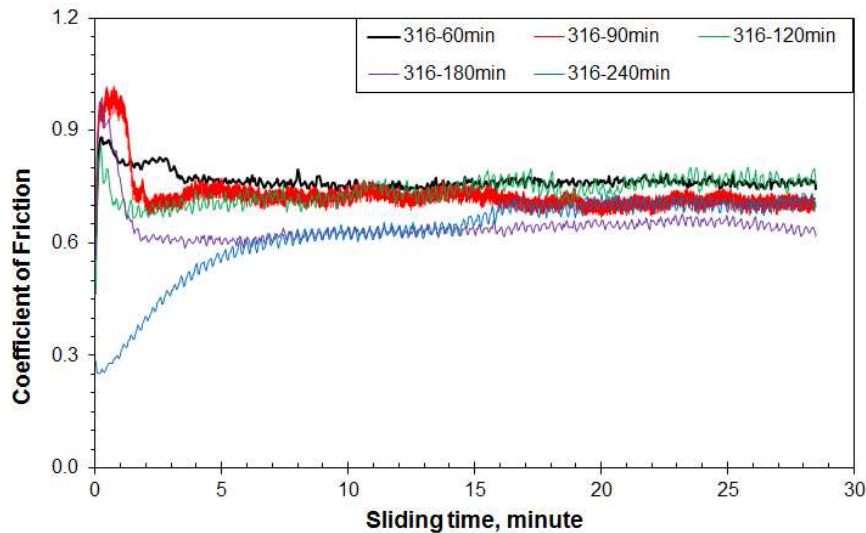

Figure 6 Friction coefficient curves of the nitrided surfaces reciprocating sliding against an alumina ball.

By averaging the friction coefficient values in the steady sliding period, namely from 5 minutes to 30 minutes, the mean friction coefficients were obtained and are listed in Table 2. The samples being nitrided for 60 to 120 minutes show friction coefficients of 0.73 - 0.76. The samples being nitrided for the longest times, 180 and 240 minutes, recorded the lowest friction coefficient values being less than 0.7. Fig. 7 shows selected optical and SEM micrographs to explain the nature of the sliding contact. After each test, the contact area of the used counterpart was found to be covered with wear debris. Fig. 7a is an optical micrograph to show a typical wear scar on the ball after most of the loose wear debris was swept off using a soft tissue. The shining bright area resulted from the sliding wear. Plenty of transferred material still attaches in the middle of the sliding contact zone, indicating strong adhesion of the wear debris to the alumina worn surface. An used counterpart ball was pressed onto a carbon based glue pad immediately after the test. Figs. 7(b-d) shows SEM observation and EDX analysis of the extracted wear debris. In Fig. 7b, the upper part exhibiting the shape of a sphere segment is a print of the core wear scar. The wear debris, as seen in Fig. 7c, show various sizes from a few micrometers to nano scale. EDX analysis reveals a high oxygen content and predominantly the constituents of the nitrided scale as well as small amount of aluminium. Moreover, the EDX analysis detected high oxygen content but no nitrogen. The result suggests firstly that the wear debris was mostly generated from the wear of the disc sample and the alumina ball also made a minor contribution. Secondly, tribo-oxidation took place as a result of the sliding friction as the tests were undertaken in air. More detailed research on the kinetics of the tribo-oxidation wear, similar to those in our previous work [32-34], is beyond the scope of this paper.

Fig. 7e is a high-magnification SEM image taken at the middle of wear track, full of fish-scale patterns and deformation grooves. The fish-scale patterns are compacted wear powders forming a thin tribofilm on the worn surface. Previous electron microscopy and spectroscopy analyses of similar tribofilms suggested that, such films could be formed through strong adhesion of wear particles to the parent worn surface and a dynamic powdering process simultaneously during the sliding tests [35-38]. Fig. 7f is a SEM image taken at a place close to the edge of the wear track of the 180 minute nitrided sample. Over the limited sliding time, the wear track seemed to have formed only partially conformal contact between the coupling surfaces. The un-worn as-nitrided areas, labelled 'II' in the image, within the wear track worked as small pools to accommodate wear debris.

The results presented in Fig. 7 suggest that, wear debris was predominantly generated from the wear of the disc surface although marginal wear of the alumina counterpart was also detected. The wear debris was engaged in the sliding contact, resulting in three-body abrasive wear. Consequently, the frictional coefficients recorded

during the tests reflected the self-mating sliding contacts between the worn surfaces and the transferred materials covering the counterpart ball.
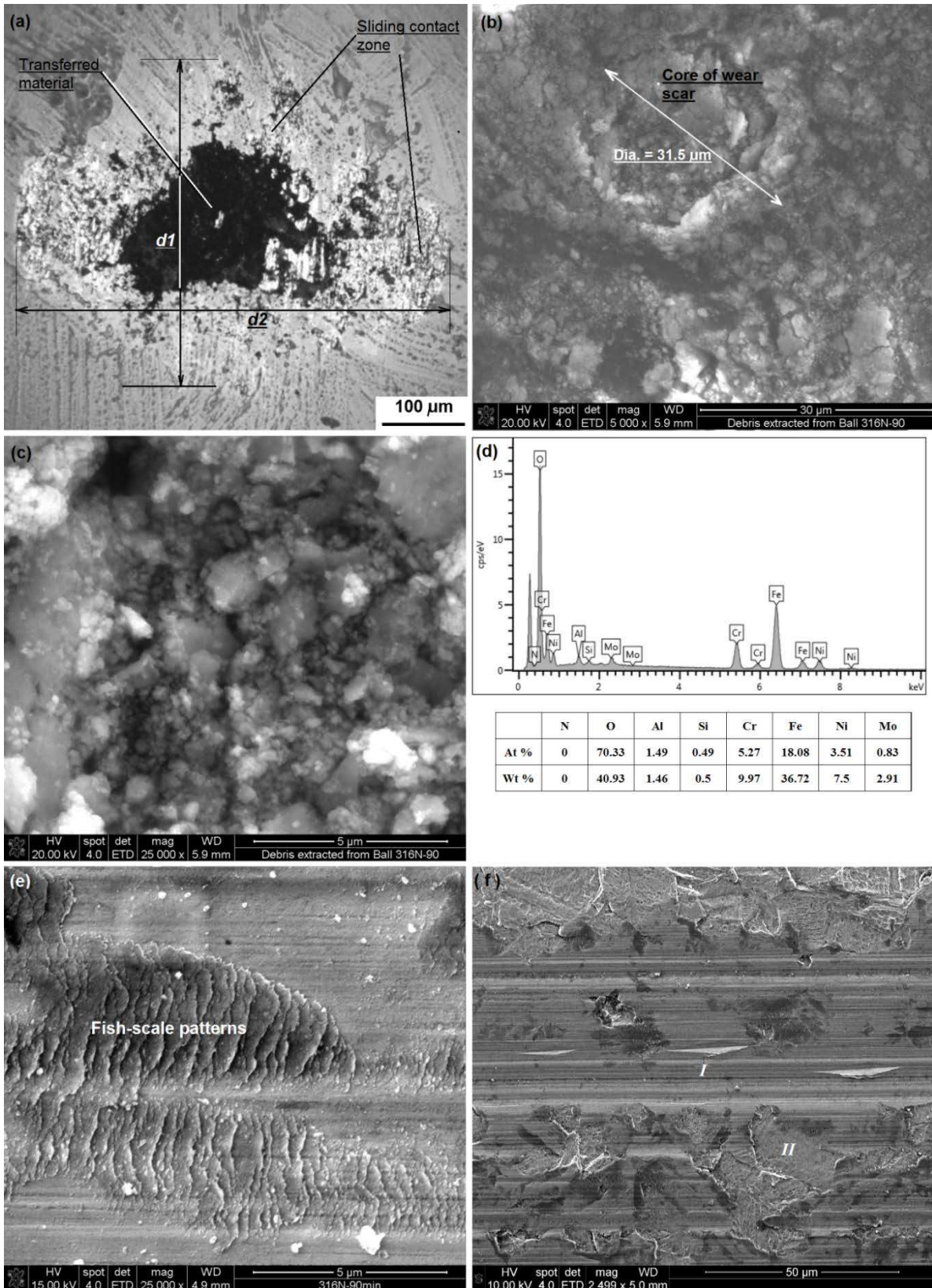

Figure 7 Microscopic analyses of the ball-on-disk sliding contacts: (a) an optical micrograph of a wear scar of the couterpart ball, where **d1** and **d2** refer to dimensions of the wear scar; (b-c) wear debris attached on the wear scar of a counterpart ball, extracted on a carbon glue pad; (d) EDX spectrum and quantitative analysis of the wear debris; (e-f) SEM images of wear track in the areas of conformal sliding contact (e) and non-conformal sliding contact (f).

3.4 Wear properties

The measured wear properties are listed in Table 2. For the wear of the nitrided disc samples, Fig. 8 shows typical cross-sectional linear profiles of the wear tracks. All the wear tracks exhibit small depths, leading to wear coefficients in the scale of 10^{-14} $m^3N^{-1}m^{-1}$. The 60 minute nitrided sample, having the single-phase γ_N structure, shows a wear coefficient of 2.07×10^{-14} $m^3N^{-1}m^{-1}$, being comparable to the 120 minute nitrided sample and lower than the 90- and 120 minute nitrided samples. The wear coefficient of the 240 minute nitrided sample is extraordinary as compared to others, which was attributed to the extremely rough surface which made its sliding behaviour different from other samples. For example, as shown in Fig. 7f, the rough disc surface resulted in a distribution of small pools to accommodate newly generated wear debris, as shown in Fig. 7f, which could have significantly extended the period of running-in sliding time before the formation of a conformal sliding contact.

Table 2 The steady-state friction coefficient and wear properties of the nitrided samples and the counterpart alumina ball

Nitriding time, min	60	90	120	180	240
Coefficient of friction	0.76	0.73	0.75	0.64	0.67
Depth of wear track, μm	1.32	1.61	1.21	1.13	0.47
Wear of disc, 10^{-14} $m^3N^{-1}m^{-1}$	2.1	3.1	2.0	6.6	0.9
Diameter of ball wear scar, μm	196	194	180	190	229
Wear of ball, 10^{-16} $m^3N^{-1}m^{-1}$	4.3	4.1	3.0	3.8	8.0

Moreover, it was suspected that the wear of the 60 minute nitrided sample might be over-estimated because the as-measured volume actually comprised both the material loss and a certain scale of plastic deformation due to the applied cross-track line profiling method. The deformation can be seen outside the wear track edges, as being arrowed in the line profile, Fig. 8. A SEM image taken at the wear track edge also shows a few cracks caused by the deformation of the soft substrate, Fig. 9b. Such deformation did not occur in other samples. Obviously, the deformation happened because the case depth of the 60 minute nitrided sample is too thin to withstand the applied sliding load. Thus, in order to obtain a wear track without pronounced substrate deformation, further sliding tests were undertaken on the same sample under the same conditions except a reduced applied load of 2.0 N. The results confirm its wear coefficients of 1.97 and 2.35×10^{-14} $m^3N^{-1}m^{-1}$ after 1,000 and 5,000 passes of reciprocating sliding respectively.
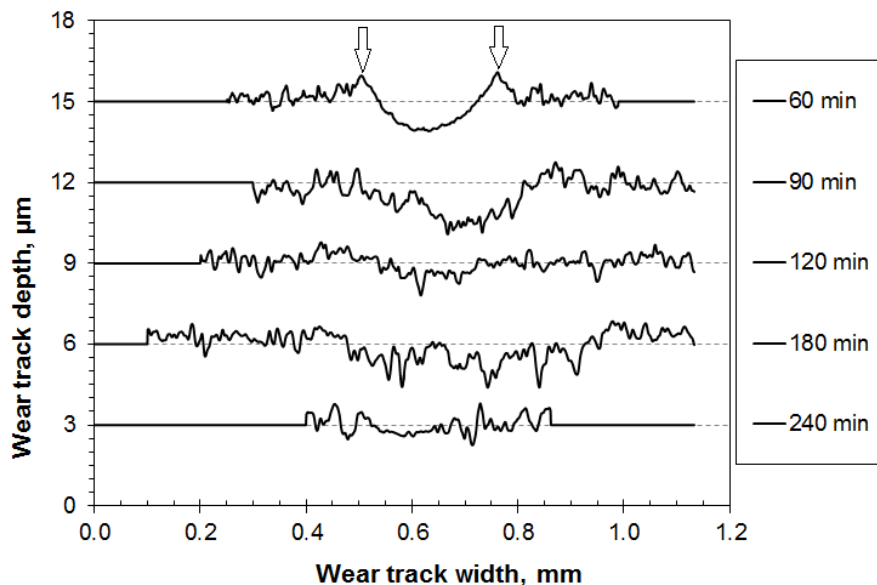

Figure 8 Linear cross-sectional profiles of wear tracks after 30 minutes of reciprocating sliding wear: the labels refer to the nitriding time of each sample.

Nitriding by 60 minutes resulted in the formation of a nitrided case of single γ_N phase and a few micrometers thick. Further increase in the nitriding time has been found to lead to remarkably increased case depth and the formation of a mixture of expanded austenite and nitride precipitates. These changes, however, did not bring about further increase in the wear resistance. This is generally consistent to the work of other researchers [19-23].

There is lack of direct comparison between current results and the data of other researchers because of the different quantitative measurements, e.g. in literature [17, 18, 20, 22, 23]. Consequently, several hard coatings grown by physical vapour deposition (PVD) have been tested at the same conditions in order to compare with the nitrided austenite steel. A TiN coating showed a wear coefficient of 1.0 - 1.4× 10^{-14} $m^3N^{-1}m^{-1}$. Other PVD coatings, including CrN, TiAlN and TiAlN/VN multilayer, showed coefficients in the scale of 10^{-15} $m^3N^{-1}m^{-1}$.

The wear coefficients of the counterpart ball have also been measured by assuming each resultant wear scar as a sphere segment. The measurement of the segment dimensions is illustrated in Fig. 7a. The wear scars all exhibited irregular ellipse shapes with the minor axis parallel to the sliding direction and the major axis perpendicular to that. Because that large amount of wear debris was engaged in the sliding, as shown in Figs. 7b-7c, and consequently resulted in the increased length in the major axis, the actual wear scar would be closer to the sphere segment with the minor axis as its diameter. Using this assumption, the wear coefficients have been estimated and listed in Table 2. The alumina counterpart ball show wear coefficients in a scale of 10^{-16} $m^3N^{-1}m^{-1}$, significantly lower than the disc samples. Moreover, it is worthwhile to note that, the 240 minute nitrided sample resulted in more pronounced wear of the counterpart. The faster wear should be attributed to the significantly increased surface roughness that the wear test took longer time before reaching its steady state of sliding friction, as shown in Fig. 6.

3.5 SEM analyses of worn surfaces

Extensive SEM observations have revealed that every resultant wear track was featured with severe ploughing deformation grooves and fish-scale patterns, as shown in Figs. 7 e-f. Plenty of wear debris has been found to adhere to the counterpart ball, Figs. 7 a-d. Due to the engaged wear debris as the third-party wear abrasives, the applied testing conditions led to three-body abrasive wear of the nitrided samples, in which the major wear features include scratches and plastic deformation, tribo-oxidation and mechanical failures associated with the high stresses. These observations are generally consistent to the worn surface features of similar nitrided cases reported by other researchers [19-22].

For the 60 minute nitrided sample, apart from the abrasion scratches, and fish-scale patterns as shown in Fig. 7e, the wear track were found to be full of transverse cracks normal to the sliding direction, Fig. 9a. Such transverse cracks did not appear in the wear tracks of thicker nitrided cases when the nitriding time was between 90 to 240 minutes. These observations suggest sufficient load bearing capacity of the thick nitrided cases whereas the nitrided case developed in the 60 minute nitrided sample was not sufficient thick to withstand the applied load. In addition to the deformation as measured in the cross-track line profile, as marked by the arrows shown in Fig. 8, the substrate deformation was also found to trigger small cracks in close vicinity of the wear track edge, Fig. 9b. Furthermore, more damages have been found in the subsurface depth of the nitrided case.

3.6 Cross-sectional SEM and TEM observations of a worn sample

To find out about microstructure changes related to the worn surface features, a cross-section specimen of the wear track of the 60 minute nitrided sample was prepared and successively observed by SEM and TEM. The method followed the author's previous work published in [36-37, 39-41]. When the longitudinal cross-sectional specimen was polished and etched on one side of the half wear track, SEM facilitated a three-dimensional view of both the worn surface and its vertical cross-section, as shown in Fig. 10. The upper part (labelled 'W') is the worn surface, where sliding grooves (labelled 'G') and narrow band of a tribofilm (labelled 'F') are visible in addition to a few cracks inside the nitrided layer. The lower part of the image is the polished and etched vertical section, consisting of the remaining nitrided layer (labelled 'N') and the austenitic substrate (labelled 'A'). More selected cross-sectional SEM images are shown in Fig. 11.

Fig. 11a is a low magnification overview of the worn surface and its longitudinal cross-section. In addition to the sliding scratches and tribofilm, several cracks can be seen within the nitrided case. Three of the worn surface cracks are linked with the grain boundaries of the substrate austenite, as marked by the arrows labelled with
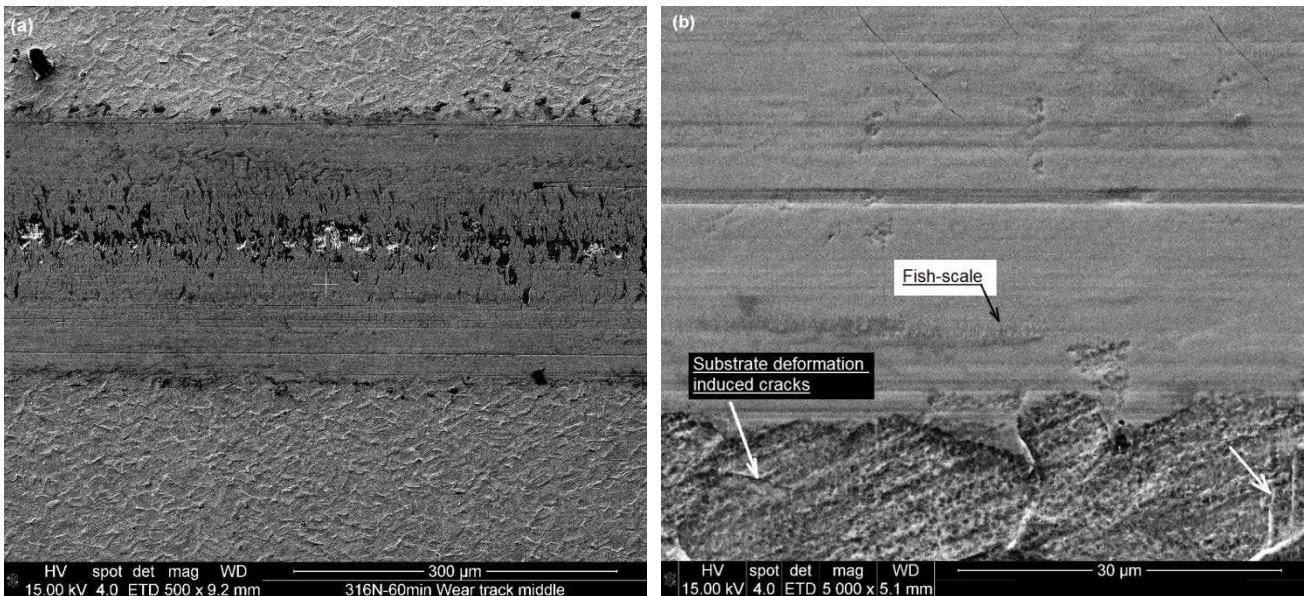
Figure 9 SEM images of the wear track edges of the 60 min nitrided samples: (a) overview of the wear track containing transverse cracks and (b) deformation grooves and fish-scale patterns in the wear track and plastic deformation in close vicinities of the wear track.
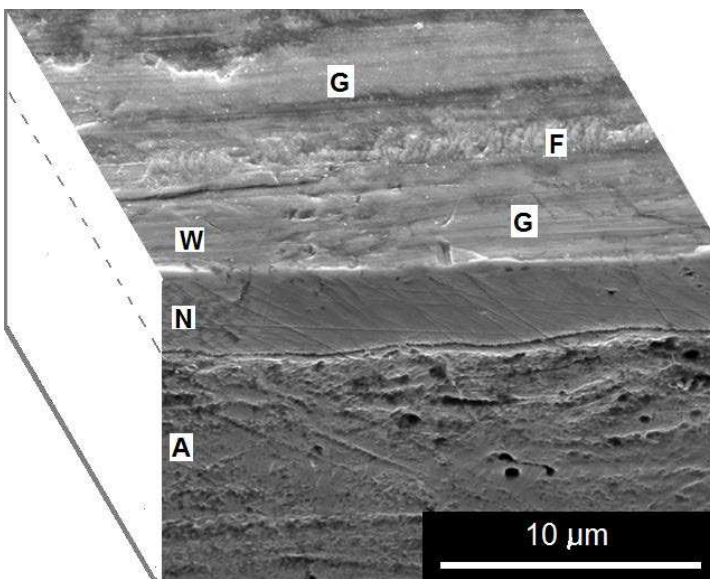

Figure 10 A schematic 3-dimentional SEM image to show the worn surface and its longitudinal cross-sections. The vertical cross-section was manually ground and polished and etched using Kailing No. 2 to show the sub-surface microstructure.

'G.B.'. Fig. 11b is a high magnification image of the highlighted middle area of Fig. 11a, to show details of the crack propagation. The two worn surface cracks have developed close to the bottom of the nitrided case, where several fine cracks are marked by arrows. In addition, the high magnification image also show that, an upmost worn surface edge exhibits less etching, within a thickness of about 0.5 μm, than the bulk of the nitrided case section. A short crack can be found in the lower part of the less-etched band, as marked by an arrow. Similar less-etched surface edge and short cracks were observed along the longitudinal sample (Fig. 11c). Such short cracks would suggest surface deformation induced delamination wear according to our previous studies of several transition metal nitride coatings [39-41]. In Fig. 11c, transverse worn surface cracks can be found to have developed in a small depth of less than 0.5 μm. Moreover, the SEM observation happened to find a large spalling pit along the prepared edge, Fig. 11d. Its internal surface shows parallel flakes.

After the longitudinal section was thinned from both sides and finally polished by ion beam milling, SEM observation was conducted again. Selected micrographs are displayed in Fig. 12 to show typical wear related features. In Fig. 12a, the black line between the upper Cu re-deposit and the main area is the top edge of the worn surface, where the Cu re-deposit was formed by the deposition of sputtered copper atoms (from the copper grid to support the specimen) as well as the steel specimen. Two pieces of delamination sheets can be seen on the
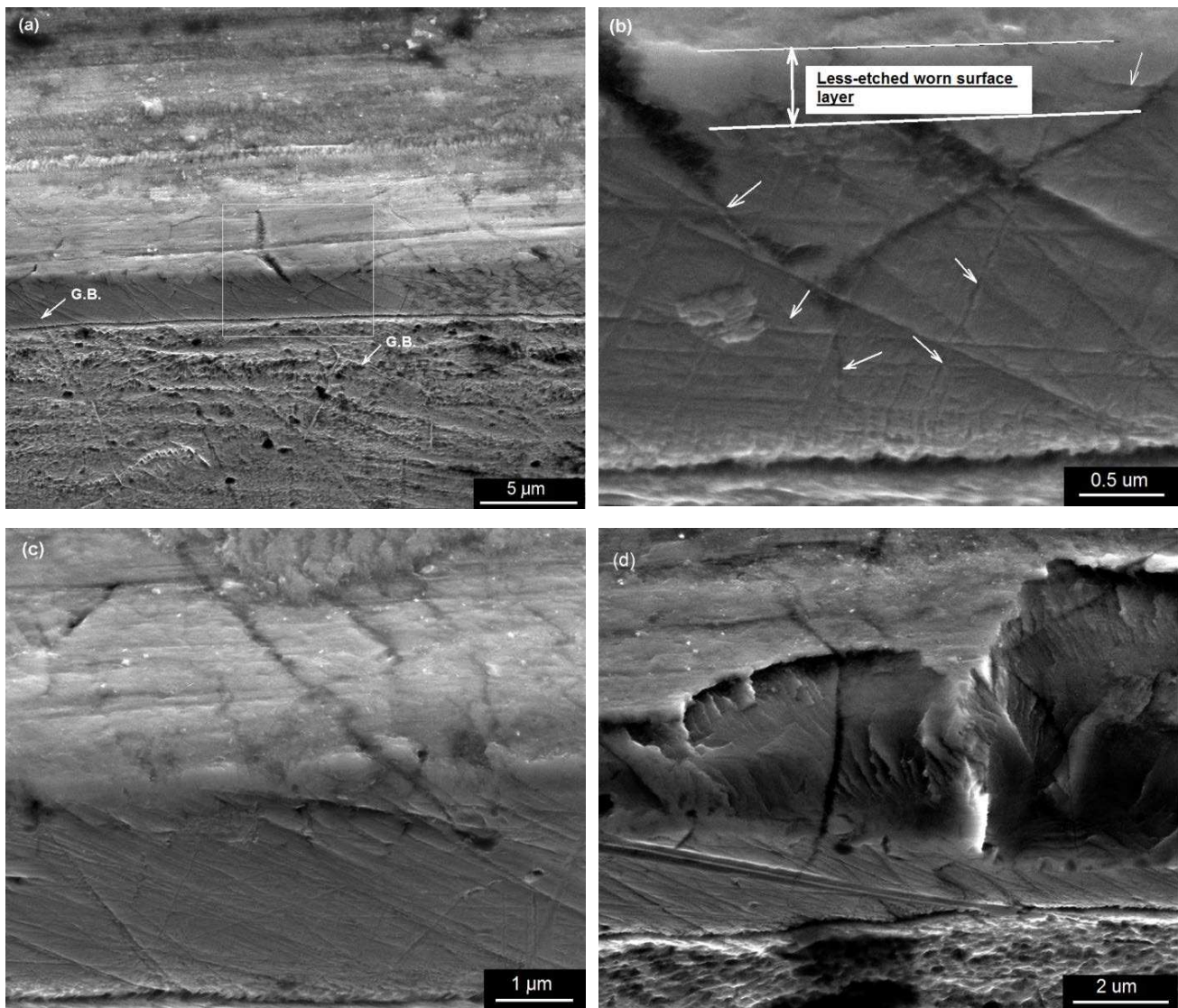
Figure 11 SEM micrographs of the worn surface and its longitudinal cross-sections.

worn surface to be about 0.3 μm thick and 1.5 μm long. The main delamination sheet is not fully detached by linking to the main body at the left hand side. A smaller sheet lies on upper left side of the main sheet. In Fig. 12b, a tribofilm attaches on the worn surface showing lower bright contrast than the main specimen area.

EDX spectroscopic analysis confirmed presence of oxygen in the tribofilm in addition to Fe, Cr and Ni, suggesting that the tribofilm is likely a multi-component oxide of the worn material. Similar oxygen-containing tribofilms have repeatedly found in our previous research on the dry sliding wear of transition metal nitride coatings [35-40]. Fig. 12c show the worn surface edge in another imaged area, where two delamination sheets were under formation through subsurface crack propagation. The depths of delamination sheets are 100 nm and 160 nm respectively. Moreover, the tribofilm exhibits various thicknesses between 30 nm and 160 nm.

Fig. 13 shows TEM bright field micrographs of the worn surface cross-section. Fig. 13a is an extremely thin area. A number of loose wear debris can be found to attach on the worn surface edge. The worn surface, in a depth of 120 – 170 nm as highlighted by the white dash line, exhibited different diffraction contrast when the specimen was tilted during the bright field observation. Similar featured layer was also found in several other edge positions when the specimen was progressively thinned and observed. Another example is shown in Fig. 13b, where the layer is 120 nm thick. The different diffraction contrast may indicate modification of the surface microstructure as a result of the plastic deformation, which is consistent to the scale of the etching insensitive layer as shown in Fig. 11. However, because the sliding was in a reciprocating manner instead of unidirectional rotary sliding, it was not expected to see deformation induced bending of grains like those features being observed in previous publications [20, 39-42]. In addition, the imaged area in Fig. 13b shows a period of open crack as a part of a large spalling pit, similar to the feature shown in Fig. 10d. Some loose wear debris, a large detached
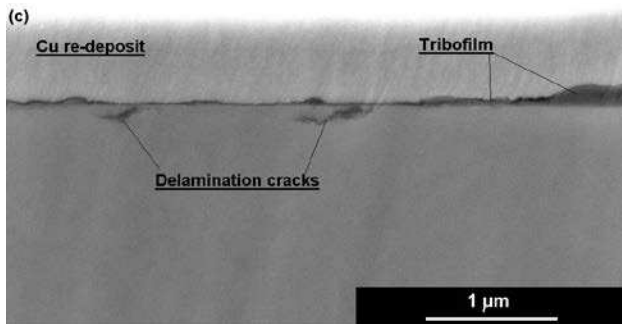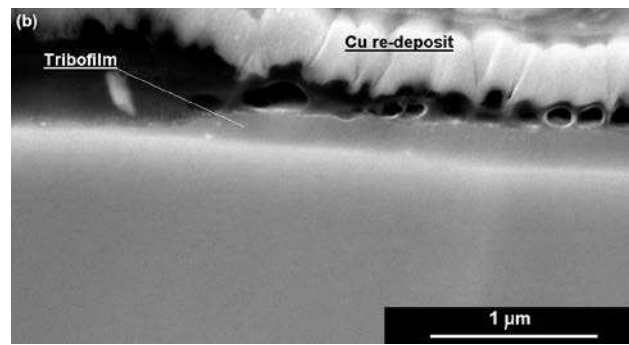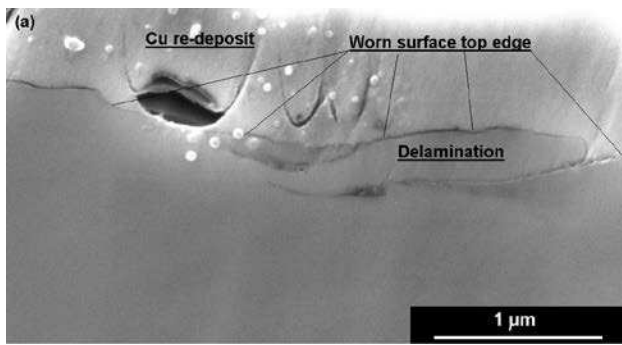
Figure 12 SEM images of the ion beam polished longitudinal cross-section of wear track of the expanded austenite γ_N layer.
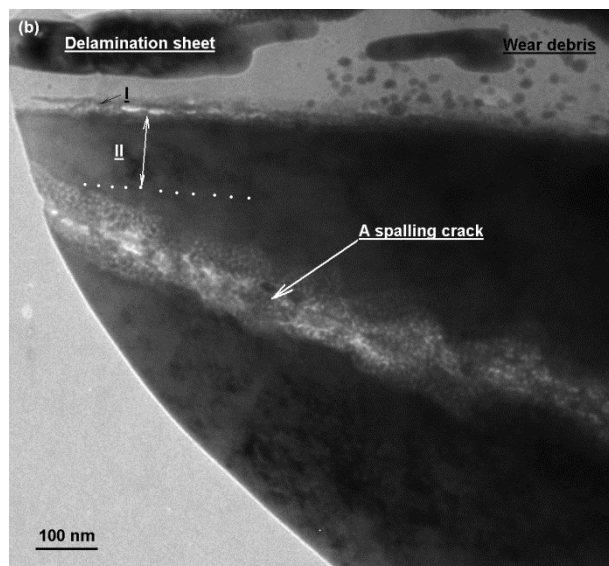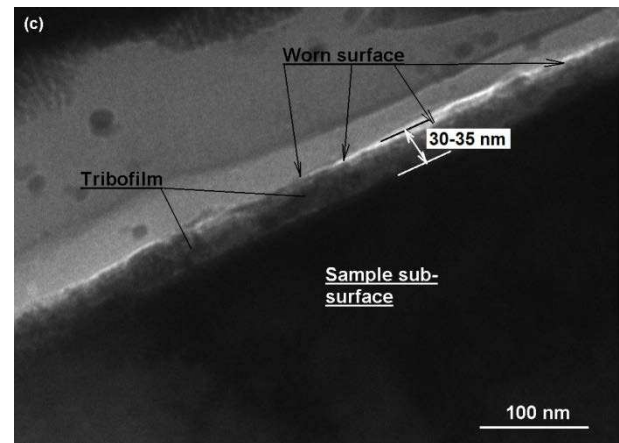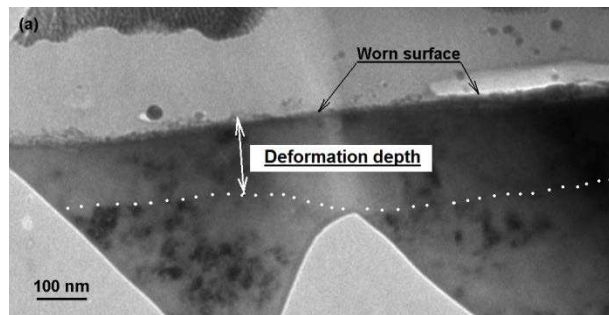

Figure 13 Cross-sectional TEM bright field images of the worn surface of expanded austenite layer, showing surface deformation, spalling crack, tribofilm, and detached wear debris.

delamination sheet and a thin sheet of tribofilm (labelled 'I') can be seen to have detached from the worn surface. Fig. 13c is an image taken in a thick area where the microstructure of the worn surface is hardly visible. However, it features a nano-scale tribofilm attached on the worn surface.

So far, the electron microscopy of worn samples has revealed the wear failure mechanisms. Firstly, the applied ball-on-disc reciprocating sliding tests resulted in three-body abrasive wear of the nitrided austenitic stainless steel, whereas the 'third body' abrasives were mostly the wear particles of the nitrided case layer instead of the alumina counterpart. Such abrasive wear led to combined mechanisms of micro-ploughing and tribo-oxidation. Because of the high hardness of the nitrided cases, the worn surface deformation was restricted to a depth of about 100 nm according to the cross-sectional FEG-SEM and TEM observations. Secondly, the self-mating sliding

contact between the wear debris attached on the ball surface and the worn surface of the disc sample resulted in a high friction coefficient. Thirdly, the currently work also reveals that a layer of single phase expanded austenite γ_N exhibited at least comparable wear resistance to the thicker and harder layers containing nitride precipitates. However, the major drawback of the γ_N layer has been the limited thickness which resulted in lower load bearing capacity. Consequently, substrate yielding resulted in the occurrence of cracking and spalling wear.

4 Conclusions

Ball-on-disc dry reciprocating sliding wear tests have been applied on austenitic stainless steel samples after being plasma nitrided for different time periods. The completed experiments lead to the following conclusions.

1) The applied ball-on-disc reciprocating sliding tests resulted in three-body abrasive wear of the nitrided austenitic stainless steel, where wear particles mostly generated from the nitrided case attached on the alumina ball surface played the role of third-party abrasives and formed self-mating sliding contact with the nitrided case surface. Such self-mating sliding contacts led to high friction coefficients.

2) The nitrided case formed after 60 minutes of nitriding treatment showed single phase structure of expanded austenite γ_N, although quantitative XRD analysis has revealed short-range clusters of CrN, Fe$_4$N and Cr$_2$N precipitates. The layer has been hardened to HK$_{0.025}$ 1212 $\pm$ 225, and consequently showed significantly reduced wear coefficient at a scale of 10^{-14} m^{3}N^{-1}m^{-1}. The wear mechanisms of the γ_N layer included abrasive wear and mild deformation in a thickness up to 100 nm, whereas the latter led to the formation of nano-delamination wear. Moreover, such a thin nitrided layer of 4.7 μm in thickness is lack of sufficient load-bearing capacity, which led to cracking and spalling failure.

3) When the nitriding time was longer than 90 minute up to 240 minutes, the obtained nitrided cases became much thicker in a range of 15 – 25 μm and showed hardness higher than HK$_{0.025}$ 2000. The increased layer thickness helped to prevent spalling cracks as a result of the increased load bearing capacity.

4) Moreover, it has been found that the applied dry sliding triggered partial decomposition of the single phase γ_N in the 60 minute nitrided sample as a result of frictional heating. In contrast, such sliding induced decomposition was not found in other samples having longer nitriding time.

Acknowledgement

References

[1] K.H. Lo, C.H. Shek, J.K.L. Lai, Recent developments in stainless steels, Mater. Sci. Eng. R65 (2009) 39-104.

[2] M.K. Lei, Phase transformation in plasma source ion nitrided austenitic stainless steel at low temperature, J. Mater. Sci. 34 (1999) 5975-5982.

[3] Y. Sun, X.Y. Li, T. Bell, X-ray diffraction characterization of low temperature plasma nitrided austenitic stainless steels, J. Mater. Sci. 34 (1999) 4793-4802.

[4] K. Ichii, K. Fujimura, T. Takase, Structure of the on-nitrided layer of 18-8 stainless steel, Technical Report Kansai University 27 (1986) 135-144.

[5] H. Dong, S-phase surface engineering of Fe-Cr, Co-Cr and Ni-Cr alloys, Int. Mater. Rev 55, 2010, 65-98.

[6] Z.L. Zhang, T. Bell, Structure and corrosion resistance of plasma nitrided stainless steel, Surf. Eng. 1 (1985) 131-136.

[7] Q. Luo, S. Yang, From micro to nano scales ☐ recent pro stainless steels, Int. J. Nanomedicine and Nanosurgery, Vol. 1.1, 2015, on-line: http://dx.doi.org/10.16966/ijnn.101 .

[8] N. Yasumaru, K. Kamachi, Nitrogen induced transformation in type 304 austenitic stainless steel, J. Japen Inst. Metals 50 (1986) 362-368.

[9] D.L. Williamson, O. Ozturk, R. Wei, P.J. Wilbur, Metastable phase formation and enhanced diffusion in f.c.c. alloys under dose, high flux nitrogen implantation at high and low ion energies, Surf. Coat. Technol. 64 (1994) 15-23.

[10] A. Leyland, D.B. Lewis, P.R. Stenenson, A. Matthews, Low temperature plasma diffusion treatment of stainless steels for improved wear resistance, Surf. Coat. Technol. 62 (1993) 608-617.

[11] K. Marchev, C.V. Cooper, J.T. Blucher, B.C. Giessen, Conditions for the formation of a martensitic single-phase compound layer in ion-nitrided 316L austenitic stainless steel, Surf. Coat. Technol. 99 (1998) 225-228.

[12] M.K. Lei, X.M. Zhu, Chemical state of nitrogen in a high nitrogen face-centred-cubic phase formed on plasma source ion nitrided austenitic stainless steel, J. Vac. Sci. Technol. 22 (2004) 2067-2070.

[13] S. Meskinis, M. Andrulevicius, V. Kopustinskas, S. Tamulevicius, XPS study of the ultrathin a-C:H films deposited onto ion beam nitrided AISI 316 steel, Appl. Surf. Sci. 249 (2005) 295-302.

[14] A. Martinavicius, G. Abrasonis, A.C. Scheinost, R. Danoix, F. Danoix, J.C. Stinville, G. Talut, C. Templier, O. Liedke, S. Gemming, W. Moller, Nitrogen interstitial diffusion induced decomposition in AISI 304L austenitic stainless steel, Acta Mater. 60 (2012) 4065-4076.

[15] A. Martinavicius, R. Danoix, M. Droue, C. Templier, B. Hannoyer, F. Danoix, Atom probe tomography characterization of nitrogen induced decomposition in low temperature plasma nitrided 304L austenitic stainless steel, Mater. Lett. 139 (2015) 153-156.

[16] X.Y. Li, Low temperature plasma nitriding of 316 stainless steel - Nature of S phase and its thermal stability, Surf. Eng. 17 (2001) 147-152.

[17] Y. Sun, T. Bell, Sliding wear characteristics of low temperature plasma nitrided 316 austenitic stainless steel, Wear 218 (1998) 34-42.

[18] C.X. Li, T. Bell, Sliding wear properties of active screen plasma nitrided 316 austenitic stainless steel, Wear 256 (2004)1144-1152.

[19] M.K. Lei, X.M. Zhu, Plasma-based low-energy ion implantation of austenitic stainless steel for improvement in wear and corrosion resistance, Surf. Coat. Technol. 193 (2005) 22-28.

[20] E.D. Las Heras, D.G. Santamaria, A. Garcia-Luis, A. Cabo, M. Brizuela, G. Ybarra, N. Mingolo, S. Bruhl, P. Corengia, Microstructure and wear behaviour of DC-pulsed plasma nitrided AISI 316L austenitic stainless steel, Plasma Porcesses& Polymers 4 (2007) S741-S745.

[21] A. Devaraju, A.E. Perumal, J. Alphonsa, S.V. Kailas, S. Venugopal, Sliding wear behaviour of plasma nitrided austenitic stainless steel type AISI 316LN in the temperature range from 25 to 400 deg C at 10 minus 4 bar, Wear 288 (2012) 17-26.

[22] L. Wang, X.L. Xu, B. Xu, Z.W. Yu, Z.K. Hei, Structure and wear resistance of ion nitride austenite stainless steel, Tribology 20 (2000) 67-69.

[23] M.C.S. Duarte, C. Godoy, J.C.A.B. Wilson, Analysis of sliding wear tests of plasma processed AISI 316L steel, Surf.Coat. Technol. 260 (2014) 316-325.

[24] S. Yang, Q. Luo, H. Sun, M. Kitchen, K. Cook, Physical and tribological properties of nitrided AISI 316 stainless steel ball, 2nd International conference on tribology and interface engineering (ICTIE2016), Chongqing, China, June 15-17, 2016.

[25] Q. Luo, K. Chi, S. Li, P. Barnard, Microstructural Stability and Lattice Misfit Characterisations of Nimonic 263, Proceedings of the ASME 2012 Pressure Vessels & Piping Division Conference (PVP2012), Vol 6, PTS A & B, p197-p206. July 15-19, 2012, Toronto, Ontario, Canada.

[26] Q. Luo, A new XRD method to quantify plate and lath martensites of hardened medium-carbon steel, J Mater Eng Perform 25, 2016, 2170-2179.

[27] F. Borgioli, A. Fossati, E. Galvenetto, T. Bacci, Glow-discharge nitriding of AISI 316L austenitic stainless steel: influence of treatment temperature, Surf Coat Technol 200 (2005) 2474-2480.

[28] O. Ozturk, S. Okur, J.P. Riviere, Structural and magnetic characterization of plasma ion nitrided layer on 316L stainless steel alloy, Nuclear Instruments and Methods in Physics Research B 267 (2009) 1540-1545.

[29] F.E. Jr. Kennedy, Thermal and thermomechanical effects in dry sliding, Wear, 100 (1984) 453-476.

[30] M.F. Ashby, J. Abulawi, H.S. Kong, Temperature maps for frictional heating in dry sliding, Tribo. Trans. 34 (1991) 577-587.

[31] E. H. Smith, R. D. Arnell, A new approach to the calculation of flash temperatures in dry, sliding contact, Tribo. Lett. 52 (2013) 407-414.

[32] Q. Luo, Origin of friction in running-in sliding wear of nitride coatings, Tribo. Lett. 37 (2010) 529-539.

[33] Q. Luo, P. Eh. Hovsepian, Transmission electron microscopy and energy dispersive X-ray spectroscopy on the worn surface of nano-structured TiAlN/VN multilayer coating, Thin Solid Films 497 (2006) 203-209.

[34] Q. Luo, Z. Zhou, W. M. Rainforth, M. Bolton, Effect of tribofilm formation on the dry sliding friction and wear properties of magnetron sputtered TiAlCrYN coatings, Tribo. Lett. 34 (2009) 113-124.

[35] Z. Zhou, W.M. Rainforth, C.C. Tan, P. Zeng, J.J. Ojeda, M.E. Romero-Gonzalez, P.Eh. Hovsepian, The role of the tribofilm and roll-like debris in the wear of nanoscale nitride PVD coatings, Wear 263 (2007) 1328-1334.

[36] Q. Luo, W.M. Rainforth, W.-D. Münz, TEM observation of wear mechanisms of TiAlCrN and TiAlN/CrN coatings grown by combined steered-arc/unbalanced magnetron deposition, Wear 225-229 (1999) 74-82.

[37] Q. Luo, W.M. Rainforth, W.-D. Münz, TEM study of the wear of TiAlN/CrNsuperlattice coatings, Script. Mater. 45 (2001) 399-404.

[38] Q. Luo, W.M. Rainforth, W.-D. Münz, Wear mechanisms of monolithic and multicomponent nitride coatings grown by combined arc etching and unbalanced magnetron sputtering, Surf. Coat. Technol. 146 –147 (2001) 430 –435.

[39] A. Devaraju, A. Elyaperumal, J. Alphonsa, S.V. Kailas, S. Venugopal, Microstructure and dry sliding wear resistance evaluation of plasma nitrided austenitic stainless steel type AISI 316LN against different sliders, Surf. Coat. Technol. 207 (2012) 406-412.

[40] X.L. Xu, L. Wang, Z.W. Yu, Z.K. Hei, Microstructural characterization of plasma nitrided austenitic stainless steel, Surf. Coat. Technol. 132 (2000) 270-274.

[41] J.C. Jiang, E.I. Meletsi, Microstructure of the nitrided layer of AISI 316 stainless steel produced by intensified plasma assisted processing, J. Appl. Phys. 88 (2000) 4026-4032.

[42] D. Stroz, M. Psoda, TEM studies of plasma nitrided austenitic stainless steel, J. Microscopy 237 (2010) 227-231.